The spectral identity of foveal cones is preserved in hue perception

Brian P. Schmidt (brian.schmidt@berkeley.edu), Alexandra E. Boehm (aeboehm@berkeley.edu), Katharina G. Foote (kfoote@berkeley.edu), and Austin Roorda (aroorda@berkeley.edu)

School of Optometry and Vision Science Graduate Group, University of California, Berkeley, USA, 94720

Abstract

Organisms are faced with the challenge of making inferences about the physical world from incomplete incoming sensory information. One strategy to combat ambiguity in this process is to combine new information with prior experiences. We investigated the strategy of combining these information sources in color vision. Single cones in human subjects were stimulated and the associated percepts were recorded. Subjects rated each flash for brightness, hue and saturation. Brightness ratings were proportional to stimulus intensity. Saturation was independent of intensity, but varied between cones. Hue, in contrast, was assigned in a stereotyped manner that was predicted by cone type. These experiments revealed that long (L) and middle (M) wavelength sensitive cones produce sensations that can be reliably distinguished on the basis of hue, but not saturation or brightness. Together, our observations support the notion that color mechanisms near the fovea contain sufficient spatial resolution to produce hue sensations in accordance with each cone's spectral type.

Introduction

Incoming sensory information is inherently noisy and ambiguous. The retinal image and the subsequent signals encoded by the photoreceptors can be interpreted infinitely many ways. Helmholtz (1924) posited that perception represents the brain's best guess about the state of the world after taking into account both the ambiguous incoming signals and prior experience. Investigating the rules through which incoming sensory signals are combined with prior evidence is an important area of brain research (Knill and Pouget, 2004). Here we studied the color appearance of light that modulates activity in a single receptor in order to elucidate the rules the visual system follows when presented with impoverished information from its primary sensory neurons. Understanding these rules will provide insight into how the visual system handles uncertainty in more naturalistic tasks as well.

A light of fixed wavelength that is sufficiently small in diameter and weak in intensity will fluctuate in appearance across presentations (Krauskopf, 1964; Krauskopf and Srebro, 1965; Otake and Cicerone, 2000). To understand why, consider a spot small enough to stimulate only a single cone. The spot will be sampled by only one of the three cone types and an individual cone is colorblind. Information about wavelength is not retained after a photoreceptor captures a photon (Rushton, 1972). The visual system computes color information by comparing relative activity across cone types. Therefore, without samples from the other two cone types, the visual system has insufficient information to unambiguously label the spot with a color. Thus, the brain must rely upon prior experience to infer the activity of the two missing classes when judging the color of the spot (Brainard et al., 2008). The reason why the spot will fluctuate from trial to trial is that the eye makes tiny movements from moment to moment. As a result of this incessant movement, the light will strike a different cone each time it is flashed on the retina. It is for this reason that a small spot

of light with a fixed wavelength fluctuates in appearance across presentations (Krauskopf, 1964; Krauskopf and Srebro, 1965; Krauskopf, 1978).

In a pioneering examination into this phenomenon, Krauskopf and Srebro (1965) observed that subjects reported one of two distinct chromatic sensations: one centered around orangish-red and the other blueish-green. They hypothesized that (1) the two perceptual distributions corresponded to two distinct detectors: L- and M-cones, respectively and that (2) white sensations arose when an L- and an M-cone were activated together. Due to technological limitations, they were unable to isolate single cones, identify the cone type targeted or repeatedly target the same cone. Thus, a conclusive test their hypothesis was not possible. More recently, Hofer et al. (2005b) improved single cone isolation with adaptive optics, which corrects for each subjects optical imperfections. Contradicting the second hypothesis of Krauskopf and Srebro (1965), they found that the majority of single-cone responses were white. However, Hofer et al. (2005b) were not able to target light to receptors of known spectral type and, therefore, could not directly relate cone activity to color reports.

Recently, we combined high-resolution eye-tracking with adaptive optics to additionally compensate for natural eye movements (Arathorn et al., 2007; Harmening et al., 2014). With this technology, we stimulated individual cones and identified their spectral type (Sabesan et al., 2015). Our results confirmed the prediction that most of the variability in chromatic percepts could be attributed to the type of cone that was targeted (Sabesan et al., 2016; Schmidt et al., 2018). On average, L-cones mediated red sensations, while M-cone trials gave rise to green or blue, depending on the background context. At a supra-threshold intensity and against a white background (Sabesan et al., 2016), a majority trials were judged white, which was consistent with the observations of Hofer et al. (2005b), but contradicted the second prediction of Krauskopf and Srebro (1965).

The discrepancy between these studies raises new questions about how the visual system parses hue and achromatic sensations from a mosaic of detectors that are individually colorblind. Firstly, do sensations from individually targeted L and M cones truly vary in saturation (amount of whiteness)? More specifically, do single-cone color percepts exist on a continuum, with each cone producing a mixture of hue and achromatic sensation (Wool et al., 2018) or is there a discrete subclass of cones wired specifically into chromatic or achromatic pathways (Neitz and Neitz, 2017)? In our prior work, subjects reported on their perception with only a single color name (Sabesan et al., 2016; Schmidt et al., 2018). The limited range of responses may have obscured more subtle variation in hue and saturation. Secondly, color and brightness perception of small spots are known to change with intensity (Kaiser, 1968; Weitzman and Kinney, 1969). However, the mechanism underlying this phenomenon is unclear. A higher luminance spot will both activate more cones and do so more strongly. We sought to understand whether individually targeted cones would systematically change in appearance – perhaps from white to colored – as the number of photons per flash was increased.

The relationship between stimulus intensity and color appearance at a cellular-scale was quantified using precise measurements of the sensation elicited by each spot. The results reveal that subjects used color terms in a stereotypical manner predicted by cone type, but largely independent of stimulus intensity. These measurements of elementary color sensations implicate the high-resolution, color-opponent parvocellular pathway in this low-level visual task.

Methods

Subjects

Three highly experienced subjects (two male, one female) between the ages of 27 and 34 participated in the study. All subjects had normal color vision and two were authors of the study. All procedures were approved by the Institutional Review Board at the University of California Berkeley and adhere to the tenets

of the Declaration of Helsinki. Informed consent was obtained from each subject before the experiments. At the start of each session, cycloplegia and mydriasis were induced with drops of 1.0% tropicamide and 2.5% phenylephrine hydrochloride ophthalmic solution.

Cone-resolved imaging and stimulation

A multi-wavelength adaptive optics scanning laser ophthalmoscope (AOSLO) was used to image and present stimuli to the retina. The objective of this study was to confine a small stimulus probe (543 nm) to targeted locations on the retina, *i.e.* individual cones. The challenges involved in targeting single cones and the technology for overcoming these challenges has been described elsewhere (Roorda et al., 2002; Arathorn et al., 2007; Harmening et al., 2012, 2014; Sincich et al., 2015) and a full consideration of the issues involved in stimulating individual receptors is beyond the scope of this paper. However, before analyzing the psychophysical results, the ability of our system to confine stimulus light to the targeted cone is worth considering. Briefly, there are three main sources of noise that causes a point source to be blurred at the retinal plane: eye-motion, optical imperfections of the eye and forward light-scatter. Forward-scatter manifests as a large, dim halo surrounding the peak of the point-spread-function. The magnitude of scatter relative to the core of the PSF has been estimated to be 1:10,000 (Hofer et al., 2005b; Harmening et al., 2014; van den Berg et al., 2010). In the dark, these scattered photons may have visual consequences. However, the presence here of photopic background raised thresholds for each cone and minimized the influence of uncontrolled scatter. Monochormatic optical imperfections were measured with a wavefront sensor (940 nm) and corrected with a deformable mirror (Roorda et al., 2002). Imaging was performed with 840 nm light, which was collected into a photo-multiplier tube through a confocal pinhole and rendered into a video stream. The video stream was registered to a reference image in real-time with a strip based cross-correlation procedure (Arathorn et al., 2007). The output of this procedure produced retinal coordinates that were used to drive an acousto-optical modulator, a high-speed optical switch, which delivered 543 nm visual stimuli to the retina whenever the raster scan passed over the targeted cell. Chromatic aberration was measured and corrected with established procedures (Harmening et al., 2012). In these experiments, a 512 x 512 pixel imaging raster subtended a 0.95° field, with a resolution of ~0.11 arcmin pixel^{-1}.

To assess the influence of the stimulus and any uncorrected blur or eye-motion, the light profile at the retinal plane was modeled and the fraction of light absorbed by the cone mosaic was subsequently computed (Harmening et al., 2014). The location of each stimulus was first determined. During each trial of the experiment, a video of the retina was recorded and the location of the stimulus in each frame was indicated with a digital mark. The digital mark was recovered from each frame after the experiment to assess how closely the actual stimulus was delivered to the desired location. The contours in the left plot of Figure 1A represent the distribution of stimulus delivery locations over all frames from all trials during an example session. The highest density of those distributions is concentrated at the center of the five targeted cones. Next, the image of each stimulus on the retina was modeled by convolving a near diffraction limited (0.05 D residual defocus) point spread function with the 3 x 3 pixel (~0.35 arcmin) stimulus. 0.05 D was chosen as a conservative estimate of uncorrected optical aberration. The contours in right panel of Figure 1A demonstrate that most of the stimulus light was confined to the targeted cone, even after accounting for uncorrected eye-movement and optical defocus. At the eccentricity (1.5°) tested in this subject (S20076), cones were separated by approximately 9-12 pixels or slightly more than one arcmin. Had cones been more tightly packed, for instance closer to the fovea, a greater fraction of the light would have been inadvertently delivered to neighboring cones.

In Figure 1B, we modeled how much light was absorbed by the targeted cone versus its nearest neighbor after taking into account the aperture of cones at this eccentricity (Harmening et al., 2014; MacLeod et al., 1992). This analysis was repeated for each trial. Of the light absorbed by the mosaic, the targeted cone captured, on average, 76.4% ($\sigma = 6.2\%$) in this subject. The next nearest neighbor captured 8.1% ($\sigma = 4.0\%$),

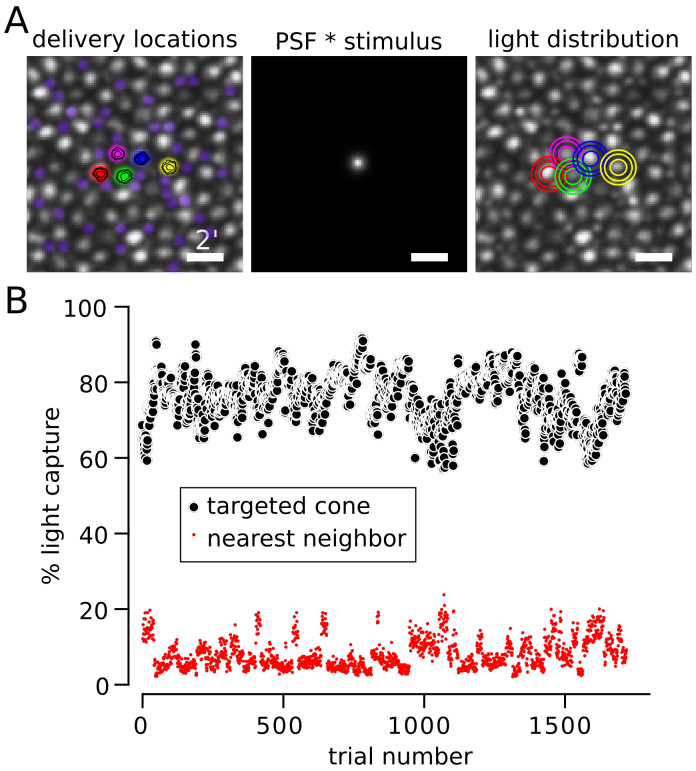

Figure 1: Targeting light to individual cones. **A.** *Left*: Delivery locations of 5 cones. The location of the stimulus was recovered on each frame of each trial (15 frames, 500 ms) and recorded. Contours indicate that delivery locations were concentrated at cone centers. Rods were pseudo-colored purple to distinguish them from cones (the larger cells). *Middle*: 3 x 3 pixel stimulus convolved with a near diffraction limited PSF (6.5 mm pupil with 0.05 diopters of defocus (Harmening et al., 2014)). *Right*: density profile of light capture in each cone computed by summing the PSF $*$ stimulus at each delivery location. For both *Left* and *Right* plots contours encompass 50, 80 and 90% of delivered light from smallest to largest. Scale bar = 2 arcmin. **B.** Estimated percentage of light captured by the targeted cone (black circles) and its nearest neighbor (red circles) during each trial. Light spread was modeled as described in **A** and each cone aperture was assumed to be Gaussian (MacLeod et al., 1992).

while the remaining 15.5% of absorbed light mostly fell on the other adjacent cones. Therefore, in theory (Harmening et al., 2014), the targeted cone in this subject absorbed 9-10 times more light than any of its neighbors. The same analysis produced similar estimates for the other two subjects (S20053: targeted cone $\mu = 67.3\%$, $\sigma = 6.6\%$, nearest neighbor $\mu = 9.9\%$, $\sigma = 3.6\%$; S20092: targeted cone $\mu = 82.1\%$, 4.2%, nearest neighbor $\mu = 6.7\%$, $\sigma = 2.9\%$. μ = mean, σ = standard deviation). The lower light capture in S20053 was predominantly driven by a higher packing density of cones at the location tested (~1°). The potential influence of greater light capture by neighboring cones is considered in the Results section.

Cone classification

A small mosaic of cones 1-2° from the fovea in each subject was selected for study. The spectral class of targeted cones were identified using densitometry (Hofer et al., 2005a; Roorda and Williams, 1999; Sabesan et al., 2015). Densitometry measurements were collected in imaging sessions separate from the psychophysical experiments. In one subject (S20092), we were unable to collect densitometry data due to time limitations.

Appearance judgments

At the start of each psychophysics session, a high SNR image was collected. From that image, the locations of 4 to 6 cones were marked. Each cone was targeted ten times at each of three intensities and an additional 10% of blank trials were added. Trials were randomly interleaved between cone locations and stimulus intensities. The subject initiated each trial with a button press. A beep indicated the start of the trial. After each flash, the subject rated the brightness of each stimulus on a scale from 0 to 5 (brightest). The subjects were given practice sessions to develop an internal criterion for assigning ratings. No reference stimulus or feedback was given. Trials that received brightness ratings above zero were also rated for hue and saturation (Gordon et al., 1994). The subject indicated the percent of red, green, blue, yellow and white contained in each stimulus using five button presses that summed to 100%. At least three full practice sessions were completed to develop familiarity with the task and the range of percepts experienced.

Cones were targeted with spots (543 nm; 500 ms; 0.35 arcmin) that varied in intensity, which was defined in arbitrary units (a.u.) of the maximum contrast achievable on our system. A flash strength with a.u. = 1 delivered approximately 3.69×10^6 photons to the cornea. Each cone location was tested at three intensities. Flash strength was chosen to sample the entire range of the frequency of seeing curve. Flash intensity is represented in linear arbitrary units relative to the maximum flash strength achievable in our system. S20053 and S20076 were tested at identical stimulus intensities. S20092 was first tested at the intensities used for the other two subjects. However, due to overall lower sensitivity to the stimulus, S20092 was subsequently tested with slightly increased intensities.

The background in these experiments was composed of four sources: the 940 nm wavefront sensing beam, the 840 nm imaging raster, the leak from 543 nm stimulation channel and an external projector. The external projector was imaged onto the subject's retina in Maxwellian view. Before each session, the subject adjusted the background of the projector until the entire mixture appeared white. The luminance was approximately 40 cd m^{-2}.

Analysis

Responses from each trial were organized by cone location and stimulus intensity. Before inclusion into the data set, each trial was analyzed for delivery error. The location of the stimulus on each frame of the recorded video was first recovered and the standard deviation of those locations was defined as the delivery error. Trials with delivery errors greater than 0.35 arcmin were discarded.

Frequency of seeing curves were computed by binarizing brightness ratings: ratings above one were seen. Frequency of seeing data was analyzed on both a cone-by-cone basis as well as in aggregate over all cones

within a single class. In both cases, the data were fit with a Weibull function, Φ, defined as:

$$\Phi = 1 - (1-g)e^{-\left(\frac{kx}{t}\right)^b} \tag{1}$$

where

$$k = -log\left(\frac{1-a}{1-g}\right)^{\frac{1}{b}} \tag{2}$$

In this parameterization of the Weibull function, g represented the performance expected during blank trials (set to 0.03 here), t was the threshold and a was the proportion correct that defined the threshold (here $a = 0.5$). The slope of the function was defined by b. Model parameters were fit to the data using a maximum likelihood routine. Only t and b were treated as free parameters.

For analysis of hue and saturation, responses were converted into a uniform appearance diagram (UAD) (Gordon et al., 1994; Abramov et al., 2009). The axes in this space were defined as $y = \frac{\bar{g}-\bar{r}}{T}$ and $x = \frac{\bar{y}-\bar{b}}{T}$, where $\bar{g}$, $\bar{r}$, $\bar{y}$, $\bar{b}$ correspond to the number of green, red, yellow, blue responses, respectively, and T was the total number of button presses. Saturation was computed as distance from the origin in city block metric (Gordon et al., 1994), *i.e* $|x| + |y|$. A purely white response falls at the origin of this space, while a purely saturated response falls along boundary where $|x| + |y| = 1$. Hue angles relative to the origin were also computed from the x and y position of each data point. $x > 0$ and $y = 0$ represented an angle of 0°. Trials with pure white responses (5 white button presses; angle = undefined) were excluded from this analysis.

Previously, we reported that the mean color reported on trials that targeted L-cones was statistically different than M-cone trials (Sabesan et al., 2016). Here, we sought to quantify the magnitude of this effect using the more subtle scaling procedure. Statistical analysis of the subjects ability to distinguish an L- versus M-cone trial was analyzed with two statistical methods. Firstly, d-prime (d') was computed:

$$d' = \frac{\mu_L - \mu_M}{\sigma_{LM}} \tag{3}$$

$$\sigma_{LM} = sqrt\frac{(N_L - 1)\sigma_L^2 + (N_M - 1)\sigma_M^2}{N_L + N_M - 2} \tag{4}$$

μL and μM were the mean hue angles for L- and M-cones, respectively. 95% confidence intervals were computed with a bootstrap procedure. Hue angle data was re-sampled with replacement 10,000 times and a distribution of d' were computed from each re-sampled data set.

As a second means of assessing the ability of subjects to distinguish cone type based on appearance, the likelihood that a given cone contained L-photopigment given a mean hue angle was computed according to Bayes theorem:

$$p(L|\theta) = \frac{p(\theta|L)p(L)}{p(\theta)} \tag{5}$$

$$p(\theta) = p(\theta|L)p(L) + p(\theta|M)p(M) \tag{6}$$

where $p(L)$ was the prior expectation that an L-cone was stimulated. $p(L)$ was set according to the fraction of L-cones (L / [L+M]) empirically measured in the subjects retina (S20053 = 0.658, S20076 = 0.667). $p(\theta|L)$ was the likelihood of θ given that an L-cone was targeted.

Unless otherwise noted, error bars represent standard error of the mean (SEM). All analyses were carried out in MATLAB. Both the analysis code and raw data will be made available on GitHub at the time of publication.

Results

Cone photoreceptors in three human volunteers were imaged and stimulated with an adaptive optics scanning laser ophthalmoscope (AOSLO). Figure 2 illustrates the psychophysical results from an example session. Five cones were selected: one M-cone and four L-cones. During each trial, a stimulus intensity were randomly selected. The subject first judged the brightness on a scale from 0 (not seen) to 5. Each subject developed his or her own criterion for brightness during practice sessions. Secondly, on trials that were seen the subject additionally judged the hue and saturation of each flash with a rating scale (Abramov et al., 2009; Gordon et al., 1994). The subject indicated the proportion of red, green, blue, yellow and white in increments of 20% (for a total of 100%). For instance, a desaturated teal might be 20% blue, 20% green and 60% white. Hue scaling data were then transformed into a uniform appearance diagram (UAD) (Figure 2D) (Abramov et al., 2009). In a UAD the x-axis indicates to the strength of yellow-blue sensations ($\frac{yellow-blue}{N_{trials}}$) and the y-axis indicates green-red bias ($\frac{green-red}{N_{trials}}$). White falls at the origin of this diagram and completely saturated responses (0% white) fall on the outer edge of plot defined by the dotted lines. Saturation was computed as the distance from the origin (in city-block metric).

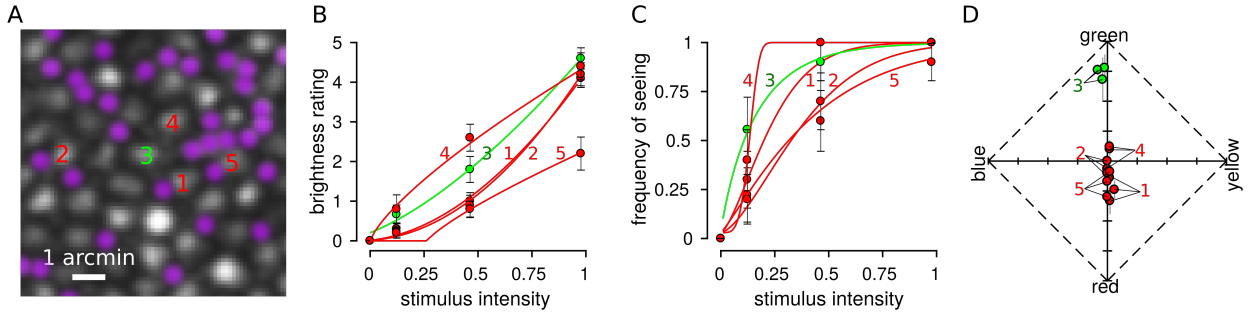

Figure 2: Hue, saturation and brightness scaling from spots targeted to single cones. **A**. Adaptive optics image from S20076 at 1.5° eccentricity. Numbers indicate the five cone centers that were selected for targeting during the experimental session. A roughly equal proportion of rods and cones are visible at this eccentricity (rods have been pseudo-colored purple). Scale bar indicates 1 arcmin. **B**. On each trial, a flash was targeted at one of the selected location and trials were randomly interleaved between the five locations. After each flash, the subject rated brightness on a scale from 0 to 5 and data were fit according to Steven's Law (Eq. 7). A brightness rating greater than zero indicated the trial was seen. **C**. Frequency of seeing data were fit with Weibull functions (Eq. 1). **D**. Subjects additionally reported the hue and saturation of the flash with a scaling procedure. The results from hue and saturation scaling from the five tested cones are plotted in a uniform appearance diagram (Abramov et al., 2009; Gordon et al., 1994). Each cone was tested at three intensities. Colors denote cone type (green = M-cones, red = L-cones.)

The cone mosaics and position of targeted cones from the three subjects are plotted in Figure 3. The location of targeted cones are indicated by the presence of a pie chart. The colors in the pie chart represent the percent each hue was reported during the scaling procedure. All three tested locations were between 1 and 2 degrees of eccentricity. The region targeted in S20053 was closest to the fovea (~1 °) and had the highest cone density.

Influence of stimulus intensity on detection and brightness

Each cone was tested ten times at three different stimulus intensities specified in arbitrary units (1 a.u. equaled the maximum value achievable in our system; ~3.69×10^6 photons/flash) and 10% of trials were

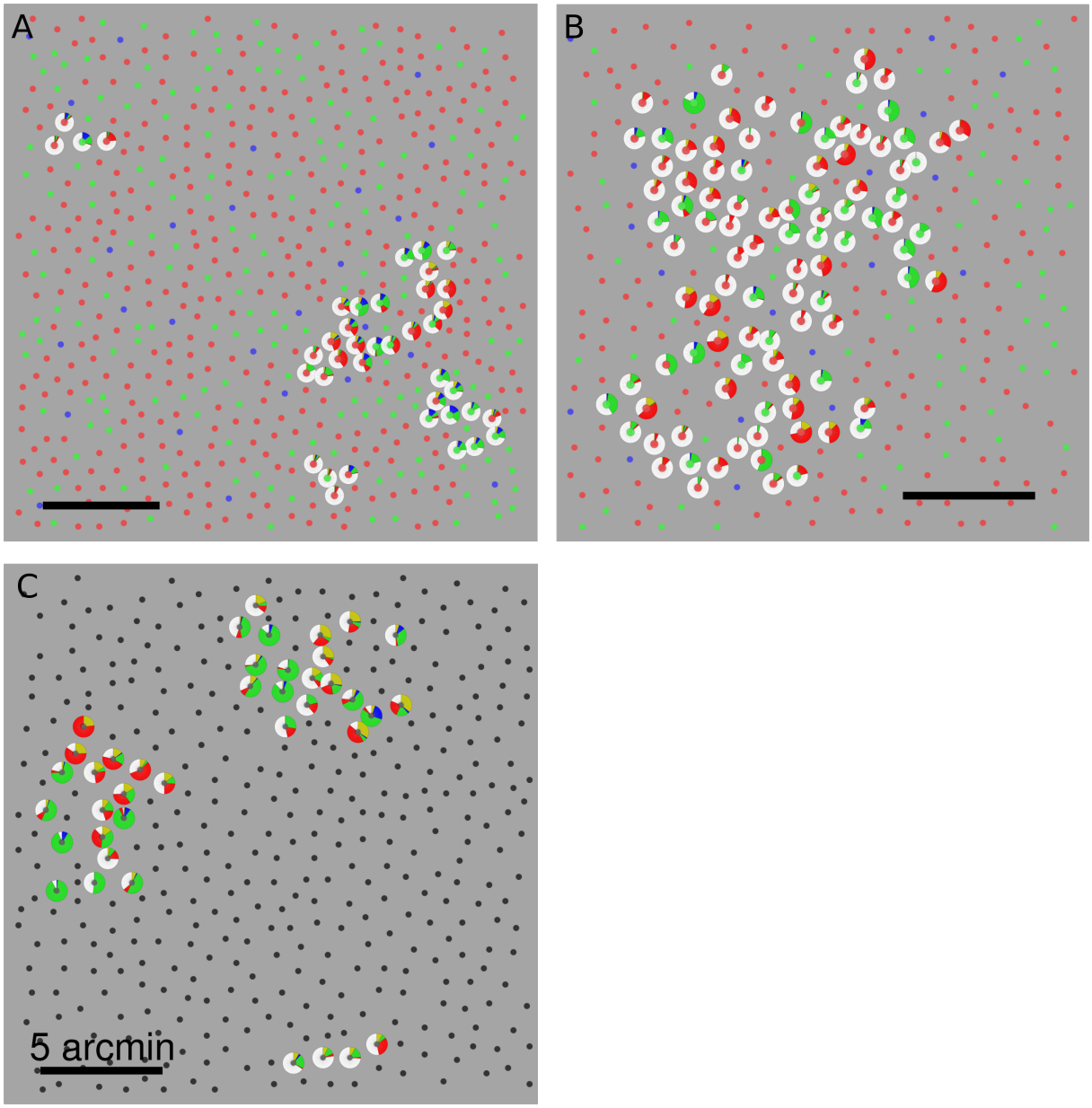

Figure 3: Tested cone locations. **A.** S20053. **B.** S20076. **C.** S20092. Targeted cones are surrounded by a pie chart that represents the fraction of times a given color was reported. Hue in the pie chart is pooled across all three stimulus intensities. The spectral class of each cone is indicated by the color. L-cones = red, M-cones = green, S-cones = blue, Unclassified = black. Scale bars indicate 5 arcmin or ~24μm.

blanks. Frequency of seeing was computed from binarized brightness ratings (ratings above 0 were seen). Figure 4 reports the FoS across our three subjects. In S20053 and S20076, L- and M-cone thresholds (defined here as 50% FoS) were similar (0.26-0.29 a.u.; Table 1). This finding is expected based on the sensitivity of L- and M-cones to our 543 nm stimulus (Stockman and Sharpe, 2000). Single cone thresholds were higher on average in S20092 (0.46 a.u.), but well within the normal range expected for healthy volunteers (Harmening et al., 2014; Bruce et al., 2015).

Thresholds were higher for stimuli delivered to S-cones, which served as a control because they are insensitive to the stimulus wavelength. 543 nm light is about 300 times less effective at activating S-cones relative to either L- or M-cones (Stockman et al., 1999). For this reason, trials targeted at S-cones should be undetectable. In cases where a spot was detected, we assume that neighboring L/M-cones absorbed some fraction of the light. Similar threshold measurements have been previously used to elucidate S-cone topography near the fovea (Williams et al., 1981). The FoS curves measured in S20076 and S20092 approximately adhere to these expectations. In S20076, S-cone FoS were significantly elevated (mean threshold = 0.85 a.u.) relative to L- and M-cones. In S20092, two (out of 62) cones had elevated thresholds (0.87 a.u.) and were purported to be S-cones. Only at the highest intensities tested did S-cone FoS increase above 50% in either subject (Figure 4B,C). In contrast, S20053 did not exhibit this behavior. S-cones thresholds were indistinguishable from L- and M-cones (0.25 a.u.). This finding may indicate that single cones were less well isolated in this subject. However, were this the case, FoS should nonetheless be systematically lower than L/M-cones due to at least a fraction of the light falling on the targeted S-cone. Another possible explanation is the tested S-cones were mis-classified and were actually L- or M-cones. We consider these two possibilities in more detail below.

Table 1: Frequency of seeing psychometric function fits

	S20076				S20053				S20092			
	N	t	b	log-likelihood	N	t	b	log-likelihood	N	t	b	log-likelihood
L-cones	77	0.261	1.616	77.08	22	0.242	2.316	16.25	60	0.464	2.185	70.41
M-cones	33	0.248	1.512	39.33	18	0.285	2.315	15.78				
S-cones	9	0.846	3.134	11.89	2	0.248	2.12	1.81	2	0.873	6.37	1.88

Data were fit according to the Weibull function defined in Eq 1. t represents the threshold for 50% frequency of seeing in arbitrary stimulus units. b controls the slope of the function.

Brightness ratings from L-, M- and S-cones are displayed in Figure 4D-F. The three subjects in our study exhibited similar gross reports of brightness ratings, which increased predictably with stimulus intensity. The dependence of intensity I on perceived brightness, ψ, was modeled according to Steven's Law (Stevens, 1966, 1961):

$$\psi = \kappa(I - I_\theta)^n \tag{7}$$

where κ represents a scaling constant, I_θ has been interpreted as a threshold (Stevens, 1961). When $n < 1$ the relationship follows a compressive non-linearity and when $n > 1$ the non-linearity becomes expansive. In S20053 and S20092, n was less than one. This finding was consistent with a compressive non-linearity that has been previously reported for brightness scaling of small spots (Stevens, 1966, 1960). The third subject (Figure 4E) was best fit by a nearly linear relationship (L-cones: $n = 1.26$; M-cones: $n = 1.11$).

Brightness ratings from S-cones were expected to follow a different model. As with FoS above, if light were properly targeted to a cone of interest, we expect a majority of the light to be coupled into that cone. For this reason S-cones should have a low FoS. Only when sufficient light is scattered into the neighboring cones will threshold be reached. Because only a minority of the light will be absorbed by those neighbors, the brightness rating should be lower than L/M-cone trials. S20076 and S20092 followed this expectation (Figure 4H&I). For

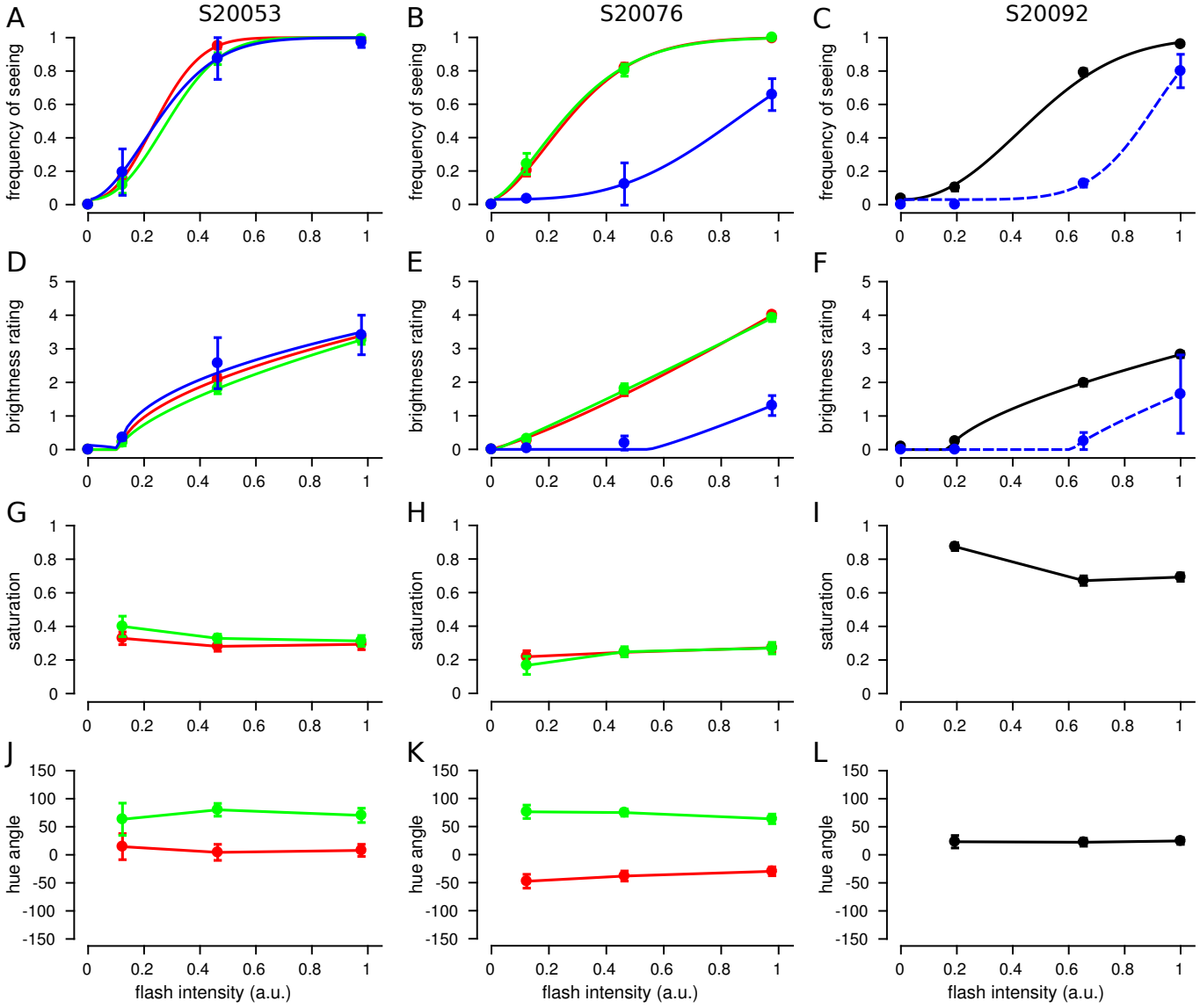

Figure 4: Brightness is dependent upon stimulus intensity, but hue and saturation are not. Color denotes spectral identity of cone targeted: red = L, green = M, blue = S, black = unclassified L or M cone, blue dotted= purported S-cones (see text for details). *Left column:* S20053. *Middle column:* S20076. *Right column:* S20092. Error bars represent SEM. **A-C:** Frequency of seeing. Data were best fit with Weibull functions (Eq 1). **D-F:** Mean brightness ratings for each subject. Data were fit with exponential Steven's Law functions (Eq 7). **G-I:** Mean saturation ratings. **J-L:** Mean hue angles.

brightness ratings from S20053, however, S-cones were no different from L/M-cone ratings. This observation is more consistent with the interpretation the two S-cones tested in this subject were mis-classified by the densitometry procedure and were actually L- or M-cones. Of the three cone types, S-cone classification is the least reliable (Roorda and Williams, 1999; Hofer et al., 2005a; Sabesan et al., 2015). Weakly reflective L- and M-cones can, in some cases, be classified as S cones.

Hue and saturation do not depend on intensity

The analysis above demonstrated that FoS and brightness ratings depended on stimulus intensity. We next asked to what degree hue and saturation ratings correlated with stimulus intensity. In Figure 2C, each cone was plotted three times (connected by a solid line) to represent the hue and saturation reported to each of the three intensities tested. It is clear from these five cones that there is some scatter in the position in UAD space across light levels. However, in comparison to brightness, stimulus intensity did not substantially influence hue and saturation ratings over the range studied (Figure 4G-L). The largest shifts in mean hue and saturation were observed between the lowest flash intensity and the highest energy stimuli. However, measurement noise was higher in low intensity conditions due to the low FoS (< 0.25 in all subjects).

The influence of stimulus intensity was also analyzed on a cone-by-cone basis. In all three subjects, hue and saturation judgments were correlated across the two highest intensities (all comparisons, all subjects: $p < 0.001$) and had slopes close to unity. Figure 5 shows the results from S20076 (*hue*: $R^2 = 0.881$, slope $= 0.85$; *saturation*: $R^2 = 0.514$, slope $= 0.81$). The results from S20053 (*hue*: $R^2 = 0.735$, slope $= 0.76$; *saturation*: $R^2 = 0.572$, slope $= 0.88$) and S20092 *hue*: $R^2 = 0.687$, slope $= 0.74$; *saturation*: $R^2 = 0.503$, slope $= 0.63$) were similar. Hue angles with saturation values below 0.1 were excluded from the analysis (29 of 187 cones). Saturation values below 0.1 were inherently noisy due to the small number of button presses that indicated the presence of a hue. Inclusion of low saturation cones did not materially change the result. Overall, these findings lend further support to the conclusion that hue and saturation judgments were largely independent of intensity.

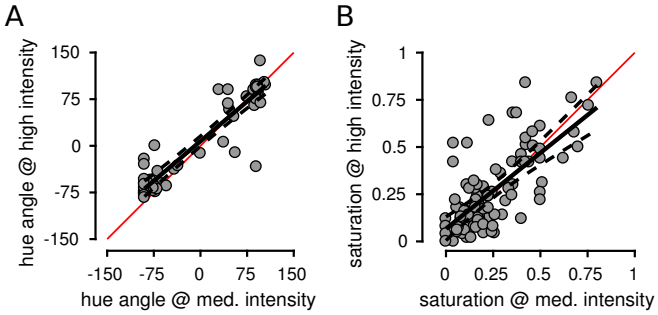

Figure 5: Hue and saturation judgments were correlated across stimulus intensities. Medium and high stimulus intensities were compared. Data are shown from S20076. Hue angles (**A**) and saturation values (**B**) were highly correlated across stimulus intensity levels.

Hue percepts correspond to cone type

Unlike stimulus intensity, the cone type targeted did impart a substantial bias on hue reports. Figure 4 reveals clear differences in the mean hue angle, μ_θ, recorded from spots targeted at L- (S20076: $\mu_\theta = -35.6 \pm 2.6°$, $N_{trials} = 793$; S20053: $\mu_\theta = 1.9 \pm 5.3°$, $N_{trials} = 326$) versus M-cones (S20076: $\mu_\theta = 74.5 \pm 2.7°$, $N_{trials} = 421$; S20053: $\mu_\theta = 80.5 \pm 4.7°$, $N_{trials} = 263$). On the other hand, saturation was not dependent on cone type (Figure 4G&H). Figure 6 represents the data across all L- and M-cones in a UAD. The appearance of

spots directed to L-cones clearly display a tendency towards reddish-yellow, while M-cone targeted spots were identified as greenish-blue in appearance. Saturation ratings were more variable between subjects. A different set of internal criteria may have been one reason for this variability. Additionally, judging the relative whiteness of a spot may be more difficult than hue, because the white background lowers achromatic contrast.

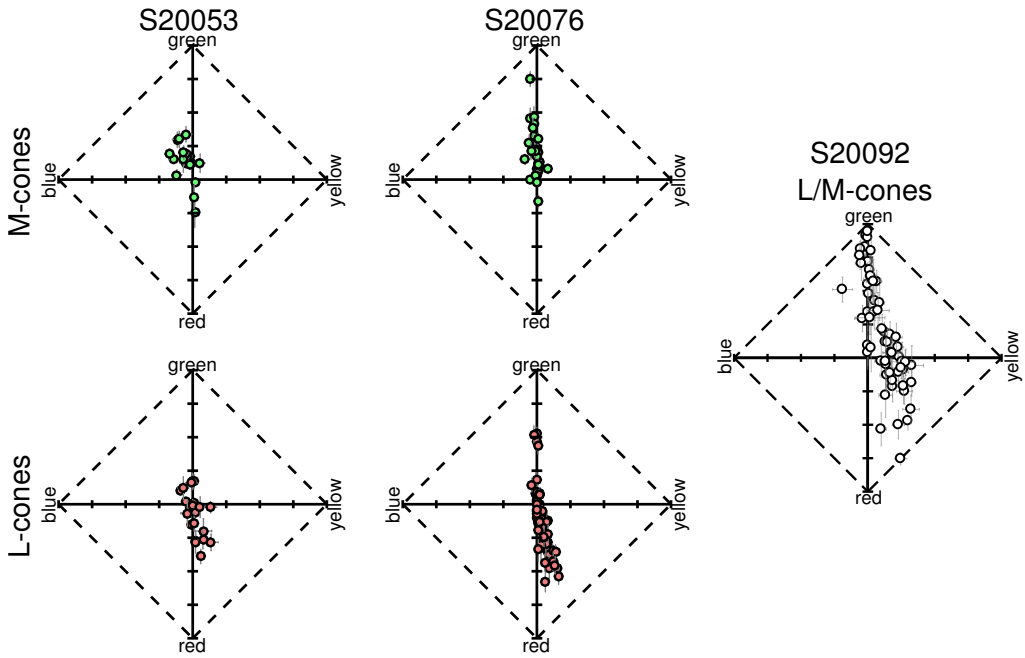

Figure 6: Variability in hue and saturation reports from targeted cones. Each dot represents the responses collected from a single cone in a uniform appearance diagram. The y-axis denotes a bias of responses towards greenness versus redness and the x-axis denotes the degree to which responses favored blueness versus yellowness. Data from L-cones are plotted in the top row and M-cones are in the bottom row. **A.** S20053. **B.** S20076. **C.** S20092.

The above analyses demonstrate that spots targeted to L- or M-cones appear perceptually different. We next assessed the extent to which the hue reported predicted the photopigment of the targeted cone. Hue angles in UAD space were first computed for all L- and M-cones. From those distributions the likelihood was found of observing a hue angle given that an L- or M-cone was targeted (Figure 7A), $p(\theta|L[M])$. In both subjects there were distinct distributions when the data were sorted based on cone type. Very few measured M-cones (3/51) produced reddish sensations (defined as $\theta < -15°$, i.e. the red side of yellow). In comparison, the distribution of L-cone hue angles was wider with a notable second peak around $75 - 90°$ (i.e. greenish). This second peak could indicate that some L-cones were mis-classified by the densitometry procedure. However, the fraction of L-cones (21/86) that yielded greenish sensations (defined as $\theta > 15°$) was higher than would be expected based on classification errors in our densitometry procedure alone (estimated to be 3-6% (Sabesan et al., 2015)). We have previously observed a similar trend (Sabesan et al., 2016).

After computing likelihood functions, the posterior probability that an L- or M-cone was targeted given the hue angle was determined following Eq 5. The results of this analysis demonstrate a clear transition around θ=15° in both subjects. When θ was less than about 10° – i.e. red or yellow – the probability that the targeted cone contained L-photopigment was very high. Larger θ values, on the other hand, were more likely to be mediated by M-cones, however, with a lower certainty. The tendency for a fraction of L-cones to produce greenish sensations produced this uncertainty.

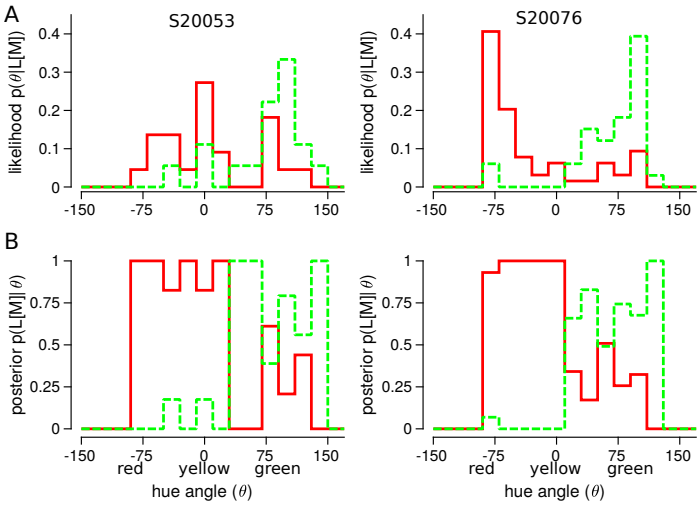

Figure 7: L- and M-cones produce distinct hue percepts. **A.** The likelihood of observing a hue angle (θ) given an L- or M-cone was targeted ($p(\theta|L[M])$). **B.** The probability an L- or M-cone was targeted given a hue angle. Computed according to Bayes rule (Eq. 5). Red lines indicate L-cones, green dashed lines represent M-cones.

Lastly, we computed how well subjects distinguished L- versus M-cone trials based on the appearance of the spot with a d' analysis. d' is a metric that indicates how distinctly two sensory stimuli are internally represented. A higher d' implies that the two stimuli generate sensory responses with greater distinction. Likelihood functions were computed for each stimulus intensity and the d' of L- and M-cone conditional likelihoods (Figure 7B) were analyzed according to Eq. 3. The results of this analysis are recorded in Table 2. In both subjects and at all intensities d' was significantly greater than zero ($p < 0.05$). This result confirms that L- and M-cones trials could be discerned based on the hue sensation they generated.

Table 2: Discriminability index (d') of hue angle distributions.

	S20053			S20076		
intensity	N	d'	95% CI	N	d'	95% CI
low	25	0.54	0.03-1.50	48	1.96	1.18-3.50
medium	40	1.28	0.65-2.19	92	1.88	1.35-3.68
high	40	1.20	0.52-2.20	95	1.61	1.10-2.32

95% confidence intervals (CI) were computed with a bootstrap procedure.

We did not find a relationship between intensity and d' (Table 2) as one might expect if noise remained constant as a stimulus intensity increased. However, in our paradigm, noise – i.e. above threshold stimulation of neighboring cones – may increase with intensity. Delivery error, forward light scatter and any uncorrected optical blur could all cause the spot to be slightly smeared at the retinal plane (Figure 1). As light intensity increases, the amount of smeared light that is absorbed by cones other than the one targeted goes up, which increases the chance that one of those neighboring cones exceeds threshold and generates a visual signal. If neighboring cones contributed to the percept in this way, they would introduced noise to the judgment of hue and d' would be expected to decrease concomitantly. However, the change observed here was small. In 20076, there was a modest, though statistically insignificant, decrease in d' as the stimulus intensity increased. This observation was consistent with the S-cone frequency of seeing analysis discussed above and further bolsters the idea that at higher stimulus intensities, the effect of any uncorrected blur from the stimulus that falls on neighboring cones is minimal. The fact that the reported percept was predicted by cone type is consistent with the targeted cone being the primary driver of the reported sensation.

Discussion

The neural computation of color depends on both relative activity across the three cone types and previous experience (Brainard, 2015; Gegenfurtner, 2003). In the case of very small spots, like the ones used here, the visual system is unable to compare stimulus driven activity across the cone classes and must rely on prior experience alone. Given this situation, one may wonder how any hue at all is perceived when light falls on only a single cone. Despite the unnatural nature of such a stimulus, subjects do often see colored spots and we report here that hue sensations were predicted based on the photopigment of the cone probed (Figure 7). These results imply that the visual system has prior knowledge of the spatial distribution of photopigment across the cone mosaic.

The presence of a spatially precise map of cone types in the human visual system may be surprising given the arrangement of the cone mosaic. There are no known molecular markers that differentiate L- from M-cones and the spatial topography of L- and M-cones near the fovea follows an approximately random distribution (Hofer et al., 2005a; Roorda and Williams, 1999; Roorda et al., 2001). During development, the expression of a single opsin gene in each cone is thought to arise through a stochastic process (Knoblauch et al., 2006; Neitz and Neitz, 2011). Furthermore, cones migrate during development towards the fovea (Hendrickson, 1994), which introduces additional spatial randomization. Thus, acquiring a spatially detailed representation of the cone mosaic is a challenge for the visual system. One possibility is that the brain learns a map of the location (Ahumada and Mulligan, 1990) and spectral identity of the cone mosaic through visual experience (Brainard, 2015; Benson et al., 2014). The intuition behind this idea is that during natural viewing the activity across a cone mosaic will be correlated in space, time and across spectral classes due to the statistics of natural scenes, eye movements and the action spectra of the photopigments. Benson et al. (2014) demonstrated that spatial and spectral correlations are theoretically sufficient to distinguish the spectral identity of cones in a mosaic. The parvocellular pathway is an obvious candidate for representing information at such fine spatial scales. Near the fovea, parvocellular (midget) ganglion cells receive input from a single cone (Kolb and Marshak, 2003; Dacey, 2000) and this private line is thought to be approximately preserved through at least the lateral geniculate nucleus (McMahon et al., 2000; Schein, 1988). In cortex, receptive fields of visual neurons increase in size (Dumoulin and Wandell, 2008; Felleman and Van Essen, 1991) and pool signals from more and more neurons. Therefore, information about cone type is unlikely to arise *de novo* at later centers.

Further insight into the neural pathways most likely involved in assigning color to activity from a single cone comes from the variability we observed in saturation judgments when cones with the same photopigment were targeted (Figure 6). Classically, small spot experiments were interpreted in the tradition of Muller's Law (Krauskopf, 1978; Krauskopf and Srebro, 1965; Krauskopf, 1964; Ingling et al., 1970; Otake and Cicerone, 2000; Hartridge, 1946). Within this framework a single neuron was thought to represent the presence or absence of a single variable, such as a red surface or an oriented bar – *i.e.* a labeled line (Muller, 1930). Accordingly, a higher firing rate was thought to indicate a redder stimulus, for example. Krauskopf and Srebro (1965) argued that the appearance of small spots detected by a single cone would carry a single chromatic sensation: light absorbed by an L-cone would appear red, while an M-cone greenish-blue. Our results were only partially consistent with that prediction. When an L-cone was targeted red/yellow was most frequently reported, while green/blue was used most often on M-cone trials (Figure 4&7). However, the present work, along with previous reports (Sabesan et al., 2016; Schmidt et al., 2018; Hofer et al., 2005b), demonstrated that cones within a spectral class often elicit different percepts (most notably saturation in our data), which contradicts the strongest form of Krauskopf and Srebro's hypothesis.

One possible explanation for this within class variability is that each cone contributes to both chromatic and achromatic channels, but with different weights (Finkelstein and Hood, 1984). A single cone contributes to the receptive field of at least 20 classes of ganglion cells that each tile the retina (Masland, 2011; Dacey, 2004). For this study (with small, near-foveal stimuli) the two numerically dominant classes of ganglion cells – the parasol and midget classes – are most relevant for consideration. Both classes are known to be

excited by single cone stimuli (Li et al., 2014; Freeman et al., 2015; Sincich et al., 2009) and project to image forming centers of the brain (Dacey, 2004). Midget ganglion cells have been proposed as the retinal substrate for red-green chromatic sensations and high acuity vision (Lee, 2011; Dacey, 2000), while parasol ganglion cells constitute a channel carrying achromatic and motion information (Manookin et al., 2018; Schiller et al., 1990). It is, therefore, possible that the variability in saturation judgments between cones of the same class may be explained by variability in the strength with which each cone feeds into these two pathways. However, were this the case, then altering the contrast (intensity) of the stimulus should favor one pathway over the other. At lower contrasts, parasol cells will be favored owing to their higher contrast response gain (Kaplan and Shapley, 1986; Shapley, 1990). At higher contrasts, the lower sensitivity midget (parvocellular) pathway will be more strongly recruited. Thus according to this idea, saturation should increase proportionally with intensity. However, we did not observe this phenomenon. Saturation judgments were relatively independent of stimulus intensity (Figure 4) and in two of the three subjects the relationship went in the opposite direction. These conclusions are further supported by previous work using small spots (Finkelstein and Hood, 1982, 1984; Finkelstein, 1988).

Alternatively, a population of neurons together may represent a property, such as color, as a probability distribution (Pouget et al., 2013). This could be accomplished if sensory input is encoded across a population of neurons with variable tuning (Ma et al., 2006; Finkelstein and Hood, 1984). Numerous authors have proposed that a representation of color space could be built in such a manner by cortical circuits that combine input from lower visual areas (Bohon et al., 2016; Kellner and Wachtler, 2013; Brainard et al., 2008; Emery et al., 2017; Finkelstein and Hood, 1984). For instance, midget ganglion cells multiplex chromatic and achromatic signals, an idea known as "double duty" (Rodieck, 1991; Dacey, 2000; Shapley, 1990). The relative strength of chromatic versus achromatic information varies between cells due to random wiring (Wool et al., 2018; Crook et al., 2011). Near the fovea, each midget cell would have an L- or M-cone in its center and variable cone weights in the surround, based on the cone types of its closest neighbors. Models explaining how randomly wired midget ganglion cells may sub-serve both chromatic and achromatic sensation have been described previously (Sabesan et al., 2016; Schmidt et al., 2014, 2016; De Valois and De Valois, 1993; Ingling Jr. and Martinez, 1983; Finkelstein, 1988; Finkelstein and Hood, 1984; Wool et al., 2018). Since each midget cell carries a unique chromatic/achromatic signature, the visual system could learn to associate different prior information with the output of each midget ganglion cell through experience (Benson et al., 2014). The color reported when a single cone is targeted with light may be a reflection of that prior experience. Finally, this theory makes the testable prediction that color reports in the peripheral retina, where the centers of midget-cell receptive fields pool signals from multiple cones (Dacey, 2000), will be less tightly predicted by the cone type stimulated.

In summary, over the range of intensities studied, the hue and, to a lesser extent, saturation of a light targeted to a single near-foveal cone was consistent from trial to trial, but brightness varied proportional to stimulus intensity. These results suggest that the visual system possesses a model of the world with enough spatial resolution to assign a meaningful hue label to spots of light that modulates the activity of only a single cone.

Acknowledgments

We thank Professor Ramkumar Sabesan for providing helpful feedback on an earlier draft of this manuscript. We are grateful for technical assistance from Dr. Nicolas Bensaid, Dr. Francesco LaRocca and Pavan Tiruveedhula. This work was supported by grants from National Eye Institute National Institute of Health (R01EY023591, F32EY027637 and T32EY704338), the Minnie Flaura Turner Memorial Fund for Impaired Vision Research and the Michael G. Harris Ezell Fellowship.

Competing interests A.R. has a patent (USPTO#7118216) assigned to the University of Houston and

the University of Rochester which is currently licensed to Boston Micromachines Corp (Watertown, MA, USA). Both he and the company stand to gain financially from the publication of these results.

References

Abramov, I., Gordon, J., and Chan, H. (2009). Color appearance: Properties of the uniform appearance diagram derived from hue and saturation scaling. *Attention, perception & psychophysics*, 71(3):632–643.

Ahumada, A. J. and Mulligan, J. B. (1990). Learning receptor positions from imperfectly known motions. *SPIE Human Vision and Electronic Imaging: Models, Methods and Applications*, 1249:124–134.

Arathorn, D. W., Yang, Q., Vogel, C. R., Zhang, Y., Tiruveedhula, P., and Roorda, A. (2007). Retinally stabilized cone-targeted stimulus delivery. *Optics Express*, 15(21):13731–44.

Benson, N. C., Manning, J. R., and Brainard, D. H. (2014). Unsupervised learning of cone spectral classes from natural images. *PLoS Computational Biology*, 10(6):e1003652.

Bohon, K. S., Hermann, K. L., Hansen, T., and Conway, B. R. (2016). Representation of perceptual color space in macaque posterior inferior temporal cortex (the V4 Complex). *eNeuro*, 3(August).

Brainard, D. H. (2015). Color and the Cone Mosaic. *Annual Review of Vision Science*, 1:1–28.

Brainard, D. H., Williams, D. R., and Hofer, H. (2008). Trichromatic reconstruction from the interleaved cone mosaic: Bayesian model and the color appearance of small spots. *Journal of Vision*, 8(5):1–23.

Bruce, K. S., Harmening, W. M., Langston, B. R., Tuten, W. S., Roorda, A., and Sincich, L. C. (2015). Normal Perceptual Sensitivity Arising From Weakly Reflective Cone Photoreceptors. *Investigative Ophthalmology & Visual Science*, 56(8):4431.

Crook, J. D., Manookin, M. B., Packer, O. S., and Dacey, D. M. (2011). Horizontal cell feedback without cone type-selective inhibition mediates "red-green" color opponency in midget ganglion cells of the primate retina. *The Journal of Neuroscience*, 31(5):1762–72.

Dacey, D. M. (2000). Parallel pathways for spectral coding in primate retina. *Annual Review of Neuroscience*, 23:743–75.

Dacey, D. M. (2004). Origins of perception: retinal ganglion cell diversity and the creation of parallel visual pathways. In Gazzaniga, M. S., editor, *The Cognitive Neurosciences III*, pages 281–301. The MIT Press, Cambridge, MA.

De Valois, R. L. and De Valois, K. K. (1993). A Multi-Stage Color Model. *Vision Research*, 33(8):1053–1065.

Dumoulin, S. O. and Wandell, B. A. (2008). Population receptive field estimates in human visual cortex. *NeuroImage*, 39(2):647–660.

Emery, K., Volbrecht, V. J., Peterzell, D. H., and Webster, M. A. (2017). Variations in normal color vision. VI. Factors underlying individual differences in hue scaling and their implications for models of color appearance. *Vision research*.

Felleman, D. J. and Van Essen, D. C. (1991). Distributed hierachical processing in the primate cerebral cortex. *Cerebral Cortex*, 1(1):1–47.

Finkelstein, M. A. (1988). Spectral tuning of opponent channels is spatially dependent. *Color Research & Application*, 13(2):106–112.

Finkelstein, M. A. and Hood, D. C. (1982). Opponent-color cells can influence detection of small, brief lights. *Vision Research*, 22(1):89–95.

Finkelstein, M. A. and Hood, D. C. (1984). Detection and discrimination of small, brief lights: variable tuning of opponent channels. *Vision research*, 24(3):175–181.

Freeman, J., Field, G. D., Li, P. H., Greschner, M., Gunning, D. E., Mathieson, K., Sher, A., Litke, A. M., Paninski, L., Simoncelli, E. P., and Chichilnisky, E. (2015). Mapping nonlinear receptive field structure in primate retina at single cone resolution. *eLife*, 4:e05241.

Gegenfurtner, K. R. (2003). Cortical mechanisms of colour vision. *Nature Reviews. Neuroscience*, 4(7):563–72.

Gordon, J., Abramov, I., and Chan, H. (1994). Describing color appearance: Hue and saturation scaling. *Perception & psychophysics*, 56(I):27–41.

Harmening, W. M., Tiruveedhula, P., Roorda, A., and Sincich, L. C. (2012). Measurement and correction of transverse chromatic offsets for multi-wavelength retinal microscopy in the living eye. *Biomedical Optics Express*, 3(9):1268–1270.

Harmening, W. M., Tuten, W. S., Roorda, A., and Sincich, L. C. (2014). Mapping the Perceptual Grain of the Human Retina. *The Journal of Neuroscience*, 34(16):5667–5677.

Hartridge, H. (1946). Colour receptors of the human fovea. *Nature*, 158:97–98.

Helmholtz, H. (1924). *Treatise on Physiological Optics.* Optical Society of America, Rochester, 1 edition.

Hendrickson, A. E. (1994). Primate Foveal Development : A Microcosm of Current Questions in Neurobiology. *Investigative Ophthalmology & Visual Science*, 35(8):3129–3133.

Hofer, H., Carroll, J., Neitz, J., Neitz, M., and Williams, D. R. (2005a). Organization of the human trichromatic cone mosaic. *The Journal of Neuroscience*, 25(42):9669–79.

Hofer, H., Singer, B., and Williams, D. R. (2005b). Different sensations from cones with the same photopigment. *Journal of Vision*, 5:444–454.

Ingling, C. R. J., Scheibner, H. M. O., and Boynton, R. M. (1970). Color naming of small foveal fields. *Vision Research*, 10:510–511.

Ingling Jr., C. R. and Martinez, E. (1983). The relationship between spectral sensitivity and spatial sensitivity for the primate r-g X-channel. *Vision Research*, 23(12):1495–1500.

Kaiser, P. K. (1968). Color Names of Very Small Fields Varying in Duration and Luminance. *Journal of the Optical Society of America*, 58(6):849.

Kaplan, E. and Shapley, R. M. (1986). The primate retina contains two types of ganglion cells, with high and low contrast sensitivity. *Proceedings of the National Academy of Sciences of the United States of America*, 83:2755–2757.

Kellner, C. J. and Wachtler, T. (2013). A distributed code for color in natural scenes derived from center-surround filtered cone signals. *Frontiers in psychology*, 4(September):661.

Knill, D. C. and Pouget, A. (2004). The Bayesian brain: The role of uncertainty in neural coding and computation. *Trends in Neurosciences*, 27(12):712–719.

Knoblauch, K., Neitz, M., and Neitz, J. (2006). An urn model of the development of L/M cone ratios in human and macaque retinas. *Visual Neuroscience*, 23(3-4):387–94.

Kolb, H. and Marshak, D. (2003). The midget pathways of the primate retina. *Documenta Ophthalmologica*, 106:67–81.

Krauskopf, J. (1964). Color Appearance of Small Stimuli and the Spatial Distribution of Color Receptors. *Journal of the Optical Society of America*, 54(9):1171.

Krauskopf, J. (1978). On Identifying Detectors. In Armington, J. C., Krauskopf, J., and Wooten, B. R., editors, *Visual Psychophysics and Physiology*, pages 283–295. Academic Press, New York.

Krauskopf, J. and Srebro, R. (1965). Spectral Sensitivity of Color Mechanisms: Derivation from Fluctuations of Color Appearance Near Threshold. *Science*, 150(3702):1477–1479.

Lee, B. B. (2011). Visual pathways and psychophysical channels in the primate. *Journal of Physiology*, 589(Pt 1):41–47.

Li, P. H., Field, G. D., Greschner, M., Ahn, D., Gunning, D. E., Mathieson, K., Sher, A., Litke, A. M., and Chichilnisky, E. (2014). Retinal Representation of the Elementary Visual Signal. *Neuron*, 81(1):130–139.

Ma, W. J., Beck, J. M., Latham, P. E., and Pouget, A. (2006). Bayesian inference with probabilistic population codes. *Nature Neuroscience*, 9(11):1432–1438.

MacLeod, D. I., Williams, D. R., and Makous, W. (1992). A visual nonlinearity fed by single cones. *Vision Research*, 32(2):347–63.

Manookin, M. B., Patterson, S. S., and Linehan, C. M. (2018). Neural Mechanisms Mediating Motion Sensitivity in Parasol Ganglion Cells of the Primate Retina. *Neuron*, pages 1–14.

Masland, R. H. (2011). Cell populations of the retina: the Proctor lecture. *Investigative Ophthalmology & Visual Science*, 52(7):4581–91.

McMahon, M. J., Lankheet, M. J. M., Lennie, P., and Williams, D. R. (2000). Fine Structure of Parvocellular Receptive Fields in the Primate Fovea Revealed by Laser Interferometry. *The Journal of Neuroscience*, 20(5):2043–2053.

Muller, G. E. (1930). *Uber Die Farbenempfindungen. Psychophys. Unters.* Barth, Leipzig.

Neitz, J. and Neitz, M. (2011). The genetics of normal and defective color vision. *Vision Research*, 51(7):633–51.

Neitz, J. and Neitz, M. (2017). Evolution of the Circuitry for Conscious Colour Vision in Primates. *Eye*, 31(2):286–300.

Otake, S. and Cicerone, C. M. (2000). L and M cone relative numerosity and red-green opponency from fovea to midperiphery in the human retina. *Journal of the Optical Society of America. A*, 17(3):615–627.

Pouget, A., Beck, J. M., Ma, W. J., and Latham, P. E. (2013). Probabilistic brains: knowns and unknowns. *Nature Neuroscience*, 16(9):1170–1178.

Rodieck, R. W. (1991). Which cells code for color? In Valberg, A. and Lee, B. B., editors, *From Pigments to Perception*, pages 83–93. Lee, Plenum Press, New York, NY.

Roorda, A., Metha, A. B., Lennie, P., and Williams, D. R. (2001). Packing arrangement of the three cone classes in primate retina. *Vision Research*, 41(10-11):1291–306.

Roorda, A., Romero-Borja, F., Donnelly, III, W., Queener, H., Hebert, T., and Campbell, M. (2002). Adaptive optics scanning laser ophthalmoscopy. *Optics Express*, 10(9):405–412.

Roorda, A. and Williams, D. R. (1999). The arrangement of the three cone classes in the living human eye. *Nature*, 397(6719):520–2.

Rushton, W. A. H. (1972). Pigments and signals in colour vision. *Journal of Physiology*, 220:1–31.

Sabesan, R., Hofer, H., and Roorda, A. (2015). Characterizing the human cone photoreceptor mosaic via dynamic photopigment densitometry. *PLoS ONE*, 10(12):e0144981.

Sabesan, R., Schmidt, B. P., Tuten, W. S., and Roorda, A. (2016). The elementary representation of spatial and color vision in the human retina. *Science Advances*, 2(9):e1600797.

Schein, S. J. (1988). Anatomy of macaque fovea and spatial densities of neurons in foveal representation. *Journal of Comparative Neurology*, 269(4):479–505.

Schiller, P. H., Logothetis, N. K., and Charles, E. R. (1990). Functions of the colour-opponent and broad-band channels of the visual system. *Nature*, 343(6253):68–70.

Schmidt, B. P., Neitz, M., and Neitz, J. (2014). Neurobiological hypothesis of color appearance and hue perception. *Journal of the Optical Society of America A*, 31(4):A195–A207.

Schmidt, B. P., Sabesan, R., Tuten, W. S., Neitz, J., and Roorda, A. (2018). Sensations from a single M-cone depend on the activity of surrounding S-cones. *bioRxiv*, page 260653.

Schmidt, B. P., Touch, P., Neitz, M., and Neitz, J. (2016). Circuitry to explain how the relative number of L and M cones shapes color experience. *Journal of Vision*, 16(18):1–17.

Shapley, R. (1990). Visual sensitivity and parallel retinocortical channels. *Annual Review of Psychology*, 41:635–658.

Sincich, L. C., Sabesan, R., Tuten, W. S., Roorda, A., and Harmening, W. M. (2015). Functional Imaging of Cone Photoreceptors. In Kremers, J., Baraas, R., and Marshal, J., editors, *Human Color Vision*, chapter 4. Springer, New York.

Sincich, L. C., Zhang, Y., Tiruveedhula, P., Horton, J. C., and Roorda, A. (2009). Resolving single cone inputs to visual receptive fields. *Nature Neuroscience*, 12(8):967–9.

Stevens, S. S. (1960). The psychophysics of sensory function. *American Scientist*, 48(2):226–253.

Stevens, S. S. (1961). To Honor Fechner and Repeal His Law. *Science*, 133(3446):80–86.

Stevens, S. S. (1966). Concerning the Measurement of Brightness. *Journal of the Optical Society of America*, 56(8):1135–1136.

Stockman, A. and Sharpe, L. T. (2000). The spectral sensitivities of the middle- and long-wavelength-sensitive cones derived from measurements in observers of known genotype. *Vision Research*, 40(13):1711–37.

Stockman, A., Sharpe, L. T., and Fach, C. C. (1999). The spectral sensitivity of the human short-wavelength sensitive cones derived from thresholds and color matches. *Vision Research*, 39:2901–2927.

van den Berg, T. J. T. P., Franssen, L., and Coppens, J. E. (2010). Ocular Media Clarity and Straylight. *Encyclopedia of Eye*, 3:173–183.

Weitzman, D. O. and Kinney, J. A. S. (1969). Effect of stimulus size, duration, and retinal location upon the appearance of color. *Journal of the Optical Society of America*, 59(5):640–643.

Williams, D. R., Macleod, D. A., and Hayhoe, M. M. (1981). Punctate sensitivity of the blue sensitive mechanism. *Vision Research*, 21:1357–1375.

Wool, L. E., Crook, J. D., Troy, J. B., Packer, O. S., Zaidi, Q., and Dacey, D. M. (2018). Nonselective wiring accounts for red-green opponency in midget ganglion cells of the primate retina. *The Journal of Neuroscience*, 38(6):1688–17.